

The size evolution of galaxy discs formed within Λ Cold Dark Matter haloes

C. Firmani^{1,2*} and V. Avila–Reese²

¹*Osservatorio Astronomico di Brera, via E. Bianchi 46, I-23807 Merate, Italy*

²*Instituto de Astronomía, Universidad Nacional Autónoma de México, A.P. 70-264, 04510, México, D.F.*

21 November 2018

ABSTRACT

By means of galaxy evolutionary models, we explore the direct consequences of the Λ Cold Dark Matter (Λ CDM) cosmogony on the size evolution of galactic discs, avoiding intentionally the introduction of intermediate (uncertain) astrophysical processes. Based on the shape of the rotation curves and guided by a simplicity criterion, we adopt an average galaxy mass baryon fraction $f_{\text{gal}} = 0.03$. In order to study general behaviors, only models with the average initial conditions are analyzed. The stellar and B -band effective radii, R_* and R_B , of individual galaxies grow significantly with time (inside-out disc formation) with laws that are weakly dependent on stellar mass, M_* , or luminosity, L_B . However, the change of R_* with z at a *fixed* M_* is slow; for $z \leq 2.5$, $R_*(M_*=\text{constant}) \propto (1+z)^{-0.4}$ for a large range of masses. On the other hand, the change of R_B with z at a *fixed* L_B is strong and it resembles the R_B decreasing law of the individual models; roughly $R_B(L_B=\text{constant}) \propto (1+z)^{-0.85}$ for $z \lesssim 0.75$, and $\propto (1+z)^{-1.1}$ for higher z 's. We find also that at $z = 0$, $R_* \propto M_*^{0.38}$ and $R_B \propto L_B^{0.40}$, remaining the slopes of these relations practically the same up to $z \approx 3$. Our model predictions are in reasonable agreement with observational inferences on the typical radius change with z of late-type galaxies more luminous (massive) than high values imposed by the selection effects. The models seem also to be consistent, within the large scatter, with the R_B and L_B values obtained from small (non complete) samples of sub- L_* late-type galaxies with available rest-frame photometric information at different z 's. The properties and evolution of the Λ CDM haloes seem to be the main drivers of galaxy disk size evolution. Nevertheless, the models reveal a potential difficulty in explaining the observed steepening of the R_B - L_B relation with respect to the R_* - M_* one, an effect related to the well established color-magnitude relation.

Key words: cosmology: theory — galaxies: evolution — galaxies: haloes — galaxies: high-redshift — galaxies: spiral

1 INTRODUCTION

The completion of multi-wavelength deep field surveys during the last years has enormously benefited the study of galaxy evolution. The analysis of galaxies with redshift known from these surveys provides valuable information about the changes with cosmic time of galaxy population properties. However, since the evolution of individual galaxies is not directly observable and because of the strong selection effects at higher redshifts, a direct interpretation of the observations is not an easy task. An adequate comparison of theoretical models with observations helps largely in this undertaking. Here we will present evolutionary models of disc galaxy formation and evolution inside growing Λ Cold Dark Matter (Λ CDM) haloes with the aim to show predictions (i) on size evolution of *individual* galaxies, and (ii) on the typical size change with redshift

z of galaxies of a fixed stellar mass, M_* , or luminosity, L . The latter results are those that can be compared with the information provided by observations.

The qualitative description of disc galaxy formation in Λ CDM haloes is based on the idea that both dark and baryonic matter acquire angular momentum by tidal torques while the perturbation is in its linear regime. The gas within the virialized halo cools and falls to its center until it attains centrifugal equilibrium forming a disc (White & Rees 1978). According to the spherical collapse model, an overdense region of mass M_h virializes with a radius R_h at the epoch z when its cumulative density overcomes $\rho_{\text{bg}}(z) \times \Delta_c(z)$, where $\rho_{\text{bg}}(z)$ is the background density at z and Δ_c is a critical value at each epoch z that depends on the cosmological model (Bryan & Norman 1998). It follows then that

$$R_h = 1.63 \left(\frac{M_h}{M_\odot} \right)^{1/3} \left(\frac{1}{(\Delta_c(z)/2) H(z)^2} \right)^{1/3} \text{ kpc}, \quad (1)$$

* E-mail: firmani@merate.mi.astro.it

where $H(z)$ is the Hubble parameter. If the disc galaxy radius is proportional to R_h , then a significant decrease of sizes with z at a fixed halo mass is expected (e.g., Mo, Mao, & White 1998; Bouwens & Silk 2002). For haloes treated as truncated isothermal spheres and assuming that an exponential disc is formed under detailed angular momentum conservation, it indeed follows that $h_d \propto \lambda R_h$ (e.g., Fall & Efstathiou 1980; Mo et al. 1998), where h_d is the disc scale length and λ is the halo spin parameter (Peebles 1969). Taking into account a Navarro-Frenk-White (NFW) density profile and including the adiabatic halo contraction due to disc formation, the latter dependence becomes $h_d \propto \lambda R_h f_c^{-1/2} f_R(\lambda, c, f_{\text{gal}})$, where c is the concentration parameter of the NFW profile, f_c is a shape-function that increases with c , $f_{\text{gal}} \equiv M_{\text{bar}}/M_h$ is the mass galaxy baryon fraction, and f_R is a function that takes into account the NFW halo adiabatic contraction for an exponential baryonic disc (Mo et al. 1998). Somerville et al. (2008) have shown that a further reduction of the change of galaxy radius with z at a fixed mass is obtained considering the fact that c decreases roughly as $(1+z)^{-1}$. These authors concluded that the observed weak change with z of typical stellar radii of disc galaxies of similar stellar masses at all redshifts agrees with the model predictions under the key assumption that λ and f_{gal} do not change with z .

The models based on the Mo et al. (1998) approach (e.g., those of Somerville et al. 2008) actually refer to a 'static' (instantaneous) population of disc galaxies at a given z ; *the models do not follow actually the individual and local evolution of the halo-galaxy system*. Besides, such models consider only baryonic discs and assume they have an exponential mass surface density distribution. The complex evolutionary processes of gas infall and local gas transformation into stars, with the consequent prediction of gas, stellar, and luminous disc properties, are beyond the scope of the mentioned models. The cosmological N-body/hydrodynamical simulations are on the other extreme of complexity. These simulations use to report the so-called 'angular momentum catastrophe' with the consequent formation of too small and compact discs (Navarro & White 1994). Such a problem seems to have been largely ameliorated in recent simulations of small volumes with a very high resolution and an appropriate tuning of sub-grid physics (e.g., Abadi et al. 2003; Governato et al. 2004, 2007; Robertson et al. 2004; Zavala, Okamoto & Frenk 2008; Scannapieco et al. 2008). Even so, the full numerical simulations do not yet allow to predict in detail the evolution of a whole population of well resolved galaxies.

From the observational side, the study of galaxy size evolution is hampered by the flux and surface brightness (SB) limits, which introduce incompleteness and selection effects in the photometric samples, particularly for those at higher redshifts. Thus, the observational inferences are yet controversial (see for recent reviews Cameron & Driver 2007; Elmegreen et al. 2007). Because magnitude and size correlate strongly, the determination of the average rest-frame surface brightnesses (SB) as a function of z has been used commonly to parametrize the evolution of galaxy sizes. In this analysis is crucial the choice of the selection and completeness functions to be applied to each z bin. In early works, an increase of the mean rest-frame B -band SB of ~ 1 mag from $z \approx 0$ to $z \sim 1$ was reported for late-type galaxies (Schade et al. 1995; Roche et al. 1998). Later on, the use of stricter completeness functions, defined for the highest z bins and imposed to the lower- z bins, showed no detectable mean SB evolution (Simard et al. 1999; Ravindranath et al. 2004). More recently, larger galaxy samples were used, and the completeness functions were estimated independently for each z bin by means of artificial galaxy simulations. As a result, a non-negligible SB or radius (at a given luminosity) evolu-

tion for luminous late-type galaxies was inferred (e.g., Bouwens & Silk 2002; Bouwens et al. 2004; Barden et al. 2005; Trujillo et al. 2006; Cameron & Driver 2007; Franx et al. 2008). Some of these samples extend up to $z \sim 3$ or even $z \sim 6$. However, as higher is z , (i) only the most luminous and highest SB galaxies of the epoch are observed, and (ii) the determination of the galaxy type becomes very uncertain.

It is important to have in mind that, likely, both radius and luminosity evolve. Therefore, is not straightforward to decipher from the sample mean SB change with z how is the size evolution of *individual* discs. Besides, the SB evolution inferences happen to be different in different rest-frame bands. Additional kinematic information (rotation velocities) certainly may help on this undertaken (see e.g., Mao, Mo & White 1998).

Given the current status of the theory and observations mentioned above, the following natural questions arise. Do the direct implications of the Λ CDM cosmogony on galactic disc evolution agree with the observational inferences? Could galaxy evolutionary models shed light on the connection between the individual evolution of discs and the sample properties inferred from photometric observations?

With the aim to answer these questions, we will use here the *semi-numerical* evolutionary approach: the assembling of haloes and the discs within them is (i) followed self-consistently (for the discs we use hydrodynamic techniques and take into account realistic descriptions for the relevant astrophysical processes, e.g., star formation, turbulence and its dissipation, stellar dynamics, gravitational instability, etc.), and (ii) for a large range of initial conditions (Avila-Reese et al. 1998; Firmani & Avila-Reese 2000 – hereafter FA2000; Avila-Reese & Firmani 2000, 2001). Alternative approaches with a similar philosophy have been developed by other authors (e.g., van den Bosch 2000; Naab & Ostriker 2006; Stringer & Benson 2007; Dutton & van den Bosch 2008). As a result of all these approaches, the models show that discs evolve inside out, and the predicted baryonic, stellar and luminous present-day scaling relations tend to be in agreement with observations (see e.g., FA00; Avila-Reese et al. 2008; Dutton & van den Bosch 2008). Here we will explore the *direct predictions of such models regarding disk size evolution*. With this aim in mind, we will not include the possible effects of intermediate (uncertain) astrophysical processes [e.g., mass outflows, long time gas cooling, active galactic nuclei (AGN) feedback].

In Section 2 a brief description of the galaxy evolutionary models and the strategy followed in this paper are presented. The results regarding disc size evolution and comparison with observational inferences are given in Section 3. Finally, a summary and the conclusions of the paper are presented in Section 4. We assume a concordance cosmology with $h = 0.7$, $\Omega_\Lambda = 0.7$, $\Omega_m = 0.3$, $\Omega_b = 0.04$, and $\sigma_8 = 0.8$.

2 THE MODEL

Our models calculate the formation and evolution of disc galaxies inside growing Λ CDM haloes, attempting to keep the underlying physics as transparent as possible. The main physical ingredients are as follows (see for details FA2000; Avila-Reese & Firmani 2000). An extended Press-Schechter approach is used to generate the halo mass accretion histories (MAHs) from the primordial Gaussian density fluctuation field. A generalized secondary infall model with elliptical orbits is applied to calculate the time-by-time virialization of the accreting mass shells (Avila-Reese et al. 1998).

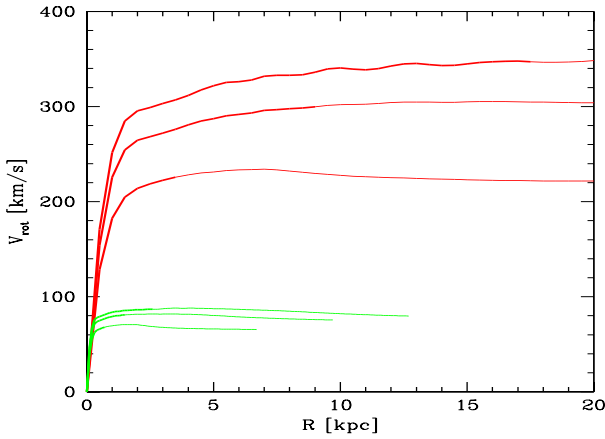


Figure 1. Total rotation curves for “central” models of $M_h = 7 \cdot 10^{10} M_\odot$ (bottom green) and $7 \cdot 10^{12} M_\odot$ (top red). From top to bottom, the curves correspond to $z = 0, 1,$ and 3 . Regions smaller than twice the effective radius (approximately one optical radius) are shown with the thick trace.

The orbit ellipticity is fixed in such a way that the structure of the Λ CDM haloes agrees well with results from cosmological N-body simulations (Avila-Reese et al. 1999; FA2000).

A constant (baryon) fraction f_{gal} of the mass of each shell is assumed to cool down in a dynamical time and form a disc layer. The accreting mass shells at the time of their virialization, t_v , are assumed to rotate rigidly with a specific angular momentum calculated as $j_{sh}(t_v) = \Delta J_h / \Delta M_h$, where Δ represents a difference between two time steps, and $J_h = \lambda_h G M_h^{5/2} / |E_h|^{1/2}$, M_h , and E_h , are the halo total angular momentum, mass, and energy respectively; λ_h is the halo spin parameter, assumed to be *constant in time*. As a result of the assembling of these mass shells, a present-day halo ends with an angular momentum distribution close to the (universal) distribution measured in N-body simulations (Bullock et al. 2001). The radial mass distribution of the layer is calculated by equating its specific angular momentum to that of its final circular orbit in centrifugal equilibrium (detailed angular momentum conservation). The superposition of these layers form a gaseous disc, which tends to be steeper in the centre and flatter at the periphery than the exponential law. The gravitational interaction of disc and inner halo during their assembly is calculated using the adiabatic invariance formalism (Blumenthal et al. 1986).

A further step is the calculation of the *stellar* surface density profile. The previously mentioned processes and the fact that star formation (SF) is less efficient at the periphery than in the centre, produces stellar discs with a nearly exponential surface density distribution, and the size mainly determined by λ_h . A cusp is present in the inner region, where the bulge is identified in observed galaxies. The disc SF at a given radius (assuming azimuthal symmetry) is triggered by the Toomre gas gravitational instability criterion and self-regulated by a balance between the energy input due to SNe and the turbulent energy dissipation in the ISM. Both such ingredients determine the gas disc height and the SF rate. This physical prescription naturally yields a Schmidt-Kennicutt-like law. The SF efficiency depends on the gas surface density determined mainly by λ_h , and on the gas infall history, which is assumed to be proportional to the halo MAH. Very simple population synthesis models

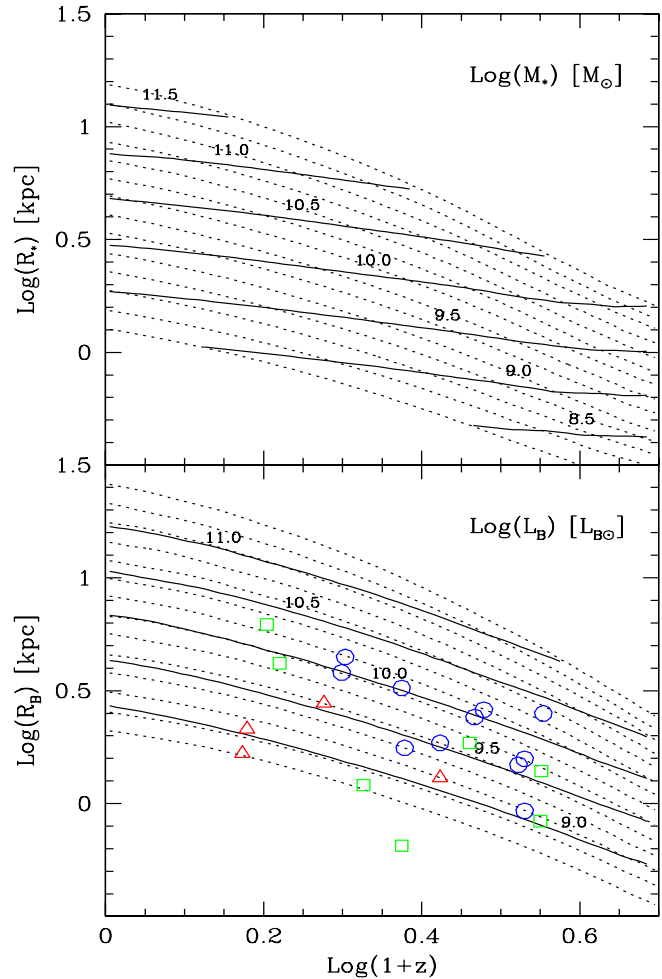


Figure 2. Dotted curves are the R_* (upper panel) and R_B (lower panel) evolutionary paths of galaxy models that at $z = 0$ have halo virial masses (from top to bottom) $M_h/M_\odot = 2.8 \cdot 10^{13}, 7.0 \cdot 10^{12}, 4.4 \cdot 10^{12}, 2.8 \cdot 10^{12}, 1.76 \cdot 10^{12}, 1.1 \cdot 10^{12}, 7.0 \cdot 10^{11}, 4.4 \cdot 10^{11}, 2.8 \cdot 10^{11}, 1.76 \cdot 10^{11}, 1.1 \cdot 10^{11},$ and $7.0 \cdot 10^{10}$ (logarithmic steps of 0.2). The solid curves connect points of constant $\text{Log} M_*$ and $\text{Log} L_B$, respectively along the individual models. The corresponding constant values are indicated inside the panels; the unities are M_\odot for M_* (upper panel), and $L_{B\odot}$ for L_B (lower panel). Symbols in the lower panel correspond to observed galaxies (Tamm & Tenjes 2006): $\text{Log} L_B < 9.5$ (red triangles), $9.5 \leq \text{Log} L_B \leq 10.0$ (green squares), and $\text{Log} L_B > 10.0$ (blue circles).

are used to calculate B - and V -band luminosities from the SF rates.

A given galaxy model is defined then by the halo MAH and λ_h , and by f_{gal} . The idea is to *keep the model as simple as possible in order to explore the direct consequences of the Λ CDM cosmogony on disc galaxy evolution*. Since we are interested here in the generic evolutionary trends, we study only the “central” models of different masses characterized by:

- the averaged MAH corresponding to the given halo mass M_h ,
- a value of $\lambda_h = 0.035$, which is close to the mean of relaxed haloes measured in numerical simulations (e.g., Bett et al. 2007),
- an average value of $f_{\text{gal}} = 0.03$

Note that all these physical ingredients have in fact dispersions (not

taken into account here) that, of course, will produce a wide scatter in the values of the output galaxy properties.

A remark has to be made about f_{gal} . Several pieces of evidence suggest values of $f_{\text{gal}} \lesssim 0.05$, though f_{gal} is expected to vary with mass, being smaller for both very low and very high luminosity galaxies. Some physical mechanisms suggested for producing such low values are SN-driven galaxy mass outflows, long gas cooling times in massive haloes, SN and AGN halo gas re-heating. Given the current uncertainties in the understanding of these processes as well as in the observational determination of the halo masses, M_{h} , we have preferred here to use a constant value for f_{gal} equal to 0.03. With such a value, our disc galaxy models agree with observed dynamical properties, mainly the approximate flatness of the rotation curves at different epochs and the present-day disc-to-total velocity ratios at the maximum of the rotation curve (see e.g., Mo et al. 1998; FA2000; Zavala et al. 2003; Gnedin et al. 2007; Dutton et al. 2007).

In Fig. 1 we plot the total rotation curve evolution ($z = 0, 1$ and 3) corresponding to our “central” models with $M_{\text{h}} = 7 \cdot 10^{10} M_{\odot}$ (bottom green) and $7 \cdot 10^{12} M_{\odot}$ (top red). The curves are nearly flat around twice the effective stellar radius R_* (indicated by the thick trace), where R_* is the radius where half of the total stellar mass M_* is contained; two R_* correspond approximately to one optical radius.

3 RESULTS

In Fig. 2, the dotted lines show the evolution of the stellar effective radius, R_* (upper panel), and the B -band effective radius, R_B (lower panel) for models with total present-day virial masses ranging from $M_{\text{h}} = 7 \cdot 10^{10} M_{\odot}$ to $M_{\text{h}} = 2.8 \cdot 10^{13} M_{\odot}$ by steps of 0.2 in logarithm. Both R_* and R_B significantly decrease with z , the decreasing being slightly steeper for the more massive galaxies. For present-day disc stellar masses ranging from $\approx 10^9$ to $\approx 10^{11} M_{\odot}$, the stellar effective radii decreases up to $z = 1$ by factors from 1.75 to 1.9, respectively; up to $z = 2$, these factors are from 2.8 to 3.2, respectively. In the B band, for the same models, which at $z = 0$ have L_B from $\approx 4.2 \cdot 10^{10}$ to $\approx 5.3 \cdot 10^8 L_{B\odot}$, the corresponding radius decreasing factors up to $z = 1$ are from 1.75 to 1.85, and up to $z = 2$, are from 2.8 to 3.3, respectively. The stellar and B -band radius evolutions tend to be similar on average, while R_B tends to be 1.4-1.6 times larger than R_* (at $z = 0$).

Along each curve in Fig. 2, M_* and L_B are also changing. We may connect the points in the different curves that have the same M_* value (upper panel) and L_B value (lower panel). These curves (solid line) show the radius that disc galaxies of a fixed M_* (L_B) have at different epochs; *this is actually the kind of information that observations can provide, rather than the individual radius evolution*. The change of radius with z along the M_* =constant curves is small. For $z < 2.5$, $R_*(M_*=\text{constant})$ decreases roughly as $(1+z)^{-0.4}$ for all the masses studied here. In the case of the L_B =constant curves, the effective radius decrease with z is strong and it resembles the decreasing law of the individual models. For $z \lesssim 0.75$, $R_B(L_B=\text{constant})$ decreases roughly as $(1+z)^{-0.85}$, and for $0.75 \lesssim z \lesssim 3$ it does as $(1+z)^{-1.1}$.

The different radius dependences on z for models in the upper and lower panels of Fig. 2 are explained basically by the differences in the evolution of M_* and L_B , which implies a significant change with z of the M_*/L_B ratio. These different evolutionary paths can also be appreciated in the $R_*(z)$ vs $M_*(z)$ and $R_B(z)$ vs $L_B(z)$ diagrams of Fig. 3 (upper and lower panels), respectively, where

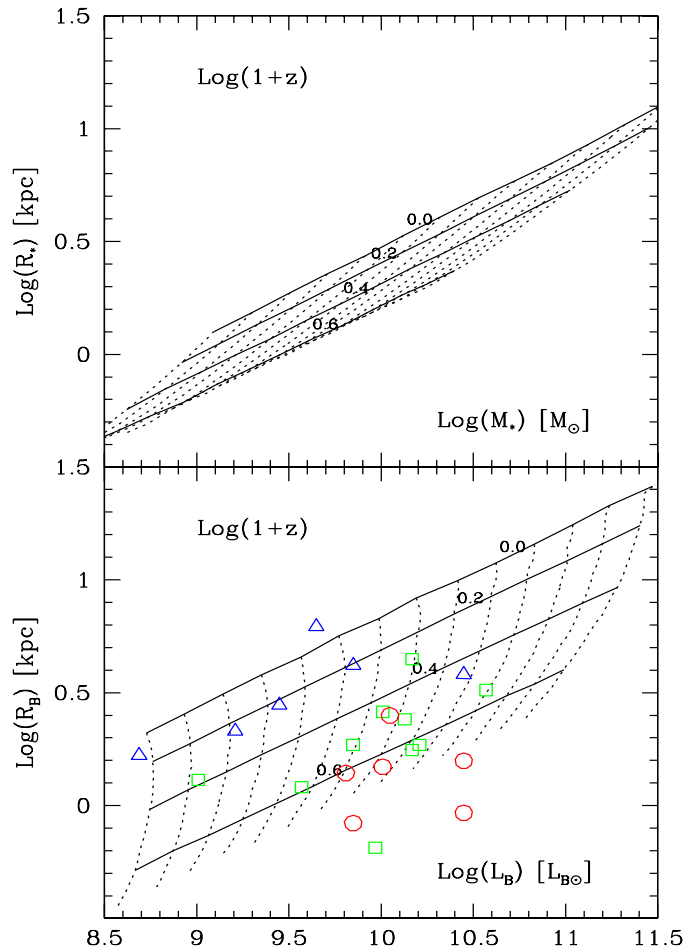


Figure 3. Relations R_*-M_* (upper panel) and R_B-L_B (lower panel) at four epochs, indicated inside the panels as $\text{Log}(1+z)$, for the “central” model galaxies studied here. Dashed lines are the evolutionary tracks of individual models. Symbols in the lower panel correspond to observed galaxies (Tamm & Tenjes 2006): $\text{Log}(1+z) < 0.3$ (blue triangles), $0.3 \leq \text{Log}(1+z) \leq 0.5$ (green squares), and $\text{Log}(1+z) > 0.5$ (red circles)

the solid lines connect models at a given z , while the dashed lines show the evolutionary tracks of individual models. At least for the “central” models studied here, we see that at $z = 0$, $R_* \propto M_*^{0.38}$ and $R_B \propto L_B^{0.40}$. Furthermore, the slopes of these correlations roughly remain the same at higher redshifts in such a way that the changes with z of the relation zero-points, $R_*(z)/M_*(z)^{0.38}$ and $R_B(z)/L_B(z)^{0.40}$, describe basically the curves of radius change at $M_*=$ constant and $L_B=$ constant, plotted in Fig. 2. Thus, our models show that using the radius change with z for a fixed mass (luminosity), or using the zero-point evolution of the radius-mass (-luminosity) relations for inferring the size evolution of galaxies, depends on how M_* and L_B do evolve.

Our results agree conceptually with those by Somerville et al. (2008). However, the predictions of these authors refer to ‘static’ populations and to baryonic discs rather than to individual evolving stellar and luminous discs (their approach does not allow to calculate gas transformation into stars). With our evolutionary models, we have generated a plot similar to the upper panel of Fig. 2 but for the baryonic effective radius and for curves of $M_{\text{bar}}=\text{constant}$. The

obtained curves follow very closely the stellar ones, showing that the radius evolution of the baryonic and stellar disc is in fact quite similar.

3.1 Model results vs observational inferences

In the lower panels of Figs. 2 and 3, the data corresponding to 22 disc galaxies with photometric z 's between 0.5 and 2.6 reported in Tamm & Tenjes (2006) are plotted. The authors used deep Near Infrared Camera and Multi-Object Spectrometer (NICMOS) J and H band images from the HDF-S field to infer rest-frame B -band photometric properties. The sample is not complete in any sense but it gives an idea of the typical B -band radii and luminosities of normal galaxies at different redshifts. In order to compare with the models, in Fig. 2 the sample is split in three luminosity ranges indicated in the figure caption. The luminosities were calculated from the absolute magnitudes reported in the paper, and both L_B and R_B were rescaled to $h = 0.7$ (they used $h = 0.65$).

In Fig. 3, the sample is split in three z ranges indicated in the figure caption. As seen in Figs. 2 and 3, the few observed galaxies seem to be consistent, within the large scatter, with the radius evolution of our models. If any, the observed galaxies at a given z and radius, seem to be on average brighter in the B band than models, specially for higher redshifts. Since L_B traces recent SF rate, such a result may be related to the so-called downsizing problem. Such difficulty appears also in the similarity between the slopes of the M_*-R_* and L_B-R_B relations showed by the models. From observations, this slope is significantly steeper for the L_B-R_B relation than for the M_*-R_* one (e.g., Avila-Reese et al. 2008), reflecting this basically the fact that our models do not reproduce the observed correlation between color and mass or luminosity. While the predicted slope in the B band seems to be only slightly shallower than observations, it is the slope of the R_*-M_* relation that is steeper than the observational inferences presented in Avila-Reese et al. (2008; see also Pizagno et al. 2005). This difference is even more dramatic at lower masses when comparing models to the observational results by Shen et al. (2003). In any case, we do not attempt to carry out a more detailed comparison of models and observations in the M_*-R_* or L_B-R_B diagrams because these relations are actually highly scattered and segregated by SB and morphological type (see e.g., Graham & Worley 2008).

In order to infer reliable estimates of the average disc radius change with z , samples at different redshift bins, complete (corrected by the selection effects) down to a given luminosity, are necessary. The changes of the luminosity and mass-size relations in the range $1 \lesssim z \lesssim 3$ of luminous (massive) field galaxy populations have been inferred recently from the Faint InfraRed Extragalactic Survey (FIRES) by Trujillo et al. (2006; see also Trujillo et al. 2004). Due to the large number of objects in their sample, the authors are able to apply a completeness function to three redshift bins. Late-type galaxies are selected as those with the Sérsic index $n \lesssim 2$. Combining the analysis of FIRES data with the results obtained by using the Galaxy Evolution from Morphologies and SEDs (GEMS) survey at $0.2 < z < 1$ (Barden et al. 2005) and tying both to the $z \sim 0$ results from SDSS (Shen et al. 2003), Trujillo et al. (2006) presented a comprehensive picture of the change with z of the mean radius and its dispersion for galaxies more luminous than $L_V \approx 3.4 \cdot 10^{10} L_{V,\odot}$ (rest-frame) or more massive than $M_* \approx 3 \cdot 10^{10} M_\odot$ at any epoch. Their results for the $n < 2$ (late-type) galaxies are reproduced in the upper (mass) and lower (luminosity) panels of Fig. 4; the error bars are the 2σ scatter on

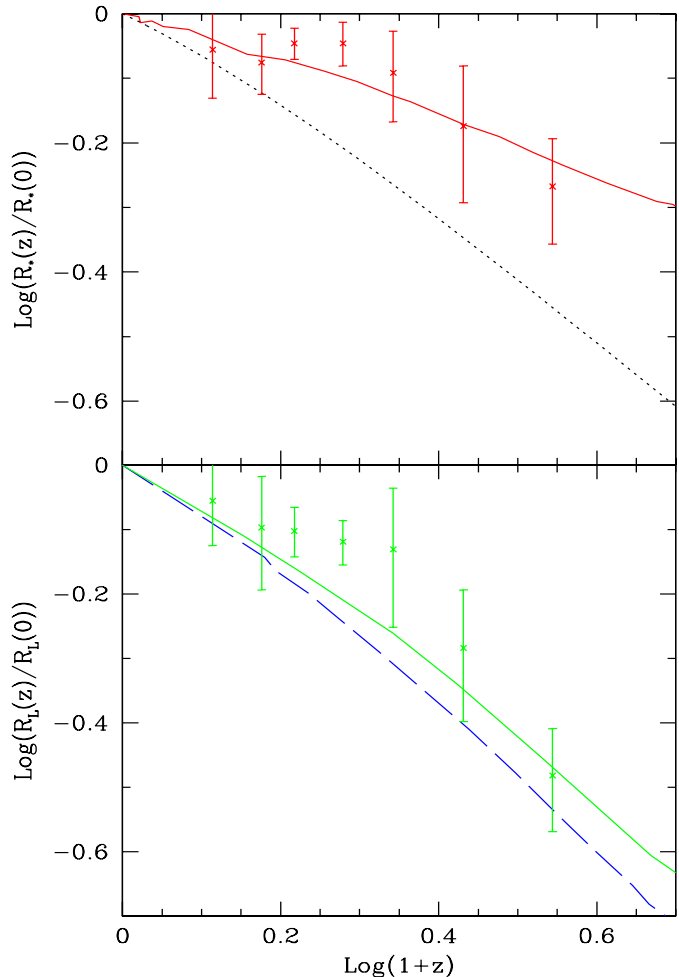


Figure 4. *Upper panel:* Crosses are the mean stellar radii normalized to the present epoch for observed disc galaxies more massive at each z than $M_* \approx 3 \cdot 10^{10} h_{70}^{-2} M_\odot$ (from Trujillo et al. 2006). The error bars are the 2σ scatter on the mean values estimated from the $\text{Log}[R_*(z)/R_*(SDSS)]$ distribution. The solid line is the R_* change normalized to $z = 0$ of model galaxies that at each z have $M_* = 3 \cdot 10^{10} M_\odot$ (the behavior of the normalized R_* change for larger values of M_* =constant. is quite similar to the one plotted here). Because the models correspond only to the "central" cases, there is not any scatter to report. The dotted line is the normalized halo radius change with z at a fixed M_h for all redshifts (eq. 1). *Lower panel:* Same as in the upper panel but in the V band, for galaxies more luminous at each z than $L_V \approx 3.4 \cdot 10^{10} h_{70}^{-2} L_{V,\odot}$ (rest-frame). The model galaxies are for $L_V = 3 \cdot 10^{10} L_{V,\odot}$ (solid line) and $L_B = 2 \cdot 10^{10} L_{B,\odot}$ (dashed line) at each z .

the mean values estimated from the $\text{Log}[R_e(z)/R_e(SDSS)]$ distribution.

The solid lines in Fig. 4 show how the normalized stellar and V band effective disc radii change with z for models that at any z have $M_* = 3 \cdot 10^{10} M_\odot$ (upper panel) and rest-frame $L_V = 3 \cdot 10^{10} L_{V,\odot}$ (lower panel), respectively. In fact, the curves are quite similar for M_* =constant in the range $10^{10} M_\odot - 3 \cdot 10^{11} M_\odot$ and L_V =constant. in the range $2 \cdot 10^{10} L_{V,\odot} - 10^{11} L_{V,\odot}$ (see Fig. 2). Thus, Fig. 4 captures the typical shape of the normalized radius change with z for galaxies of the same mass or luminosity at different z 's. Some observations suggest that the normalized R_* change with z could be slightly steeper for the largest masses (Barden et al. 2005; Trujillo

et al. 2006; Franx et al. 2008). However, any possible dependence with mass is within the large scatter of the R_* - M_* correlations at different z 's and the observational uncertainties. Besides, at higher z 's the samples are probably biased to observe earlier-type galaxies since they strongly emit in UV at their early formation phases; and early-type galaxies are more compact than late-type galaxies.

The dotted line in the upper panel shows the redshift change of the normalized halo virial radius, R_h given by eq. (1). Our evolutionary models show that the relative radius change with z for a fixed disc stellar mass is much slower than in the case of dark matter haloes. For completeness, we also plot in the lower panel of Fig. 4, models in the B band, for rest-frame $L_B = 2 \cdot 10^{10} L_{B,\odot}$ (dashed line). The sequence is clear: the decrease of the normalized radius with z for a fixed luminosity (or stellar mass, which is closely related to a K band) is steeper as the pass-band is bluer.

We did not include in our models the possible cooling flow regime for gas infall due to cooling times longer than the dynamical time in massive haloes. By truncating the late infall of high-angular momentum gas, the disc radius increasing is expected to be halted. Detailed calculations (e.g., Dutton & van den Bosch 2008) show that gas infall is truncated at $z \approx 0$ for haloes of virial mass $M_h \approx 6 \cdot 10^{11} M_\odot$ (corresponding to $M_* \approx 10^{10} M_\odot$ and $L_V \approx 7 \cdot 10^9 L_{V,\odot}$ in the case of the models presented here). As the halo is more massive than this value, the truncation of gas infall starts earlier. Therefore, the long cooling time in massive haloes is expected to work in the direction of flattening the late radius change with z of galaxies of masses $M_* > 10^{10} M_\odot$ (or $L_V > 7 \cdot 10^9 L_{V,\odot}$), approaching even more models to observations in Fig. 4. We did not include either the possible feedback mass outflow mechanism, which introduces a decrease of f_{gal} as M_h is smaller. Such a dependence is expected to produce a flattening of the R_* - M_* relation at lower masses (Shen et al. 2003; Somerville et al. 2008), improving perhaps the comparison with observations in that regards this relation.

4 CONCLUSIONS

We have presented results on disc size change with redshift obtained by means of galaxy *evolutionary* models within the context of the Λ CDM cosmogony. Under the assumption of detailed angular momentum conservation, discs are formed in centrifugal equilibrium inside growing Λ CDM virialized haloes, taking into account the central halo (adiabatic) contraction due to the disc gravitational drag. The gas infall rate is assumed to be a constant fraction f_{gal} of the halo mass accretion rate. The hydrodynamic equations for the gaseous and stellar discs are resolved coupled under the assumption of azimuthal symmetry and vertical virial equilibrium. The SF is triggered by the Toomre instability criterion and self-regulated by an energy balance between SN energy input and ISM turbulent dissipation. The driving parameters of the models are the halo MAH, the spin parameter λ_h , and the mass galaxy fraction, f_{gal} .

Since our main goal was to explore the general behavior of disc size evolution, here we took into account only ‘‘central’’ models constructed with the average MAH corresponding to a given M_h , a value of $\lambda_h = 0.035$ close to its mean, and a global average value for $f_{\text{gal}}=0.03$; both λ_h and f_{gal} are further assumed to be constant in time. *We avoided the introduction of some (uncertain) astrophysical processes in order to explore in a transparent fashion the direct consequences of the Λ CDM cosmogony on disc size (and mass/luminosity) evolution*; the assumed value of f_{gal} is based on

the success of the models to produce nearly flat rotation curves and realistic disc-to-halo velocity ratios. Our main conclusions are:

- The model stellar and B luminosity disc effective radii significantly decrease with z (inside-out disc formation), the decreasing at high z 's being slightly steeper for the more massive galaxies (Fig. 2). The radius growth in the B band is only slightly steeper than the one of the stellar disc, and at $z = 0$, R_B is 1.4-1.6 times larger than R_* .

- The change of R_* with z at a fixed M_* –this is the kind of information able to infer from the observations– is much weaker than the radius evolution of the individual models (Fig. 2). For $z \lesssim 2.5$, $R_*(M_*=\text{const}) \propto (1+z)^{-0.4}$ for all the masses studied here. This law is much shallower than the one corresponding to the haloes, which was widely used in the literature for comparisons with observations. On the other hand, in the B band, the decrease of $R_B(L_B=\text{const})$ with z is strong and it resembles the radius decreasing law of the individual models. For $z \lesssim 0.75$, $R_B(L_B=\text{const}) \propto (1+z)^{-0.85}$, and for $0.75 \lesssim z \lesssim 3$, $R_B(L_B=\text{const}) \propto (1+z)^{-1.1}$. Since the radius growth of the stellar and B band discs is similar for the individual models, the difference in the radius change with z for models of the same M_* and L_B at all z 's is basically due to the differences in the individual evolutionary paths of M_* and L_B .

- The slopes of the R_* - M_* and R_B - L_B relations remain practically the same since $z = 0$ up to $z = 3$; these slopes at $z = 0$ are 0.38 and 0.42, respectively (Fig. 3). Therefore, the changes with z of the relations zero-points, $R_*(z)/M_*(z)^{0.38}$ and $R_B(z)/L_B(z)^{0.40}$, describe basically the radius change curves at $M_*=$ constant and $L_B =$ constant shown in Fig. 2. The similarity in the slopes of both relations disagrees with observational inferences at $z = 0$, which show a significant steepening from the stellar to the B band relation. Such a behavior is related to the well known color-magnitude (mass) relation, which our models do not reproduce.

- Model predictions are in reasonable agreement with observational inferences of the typical R_* and R_V change with z for disc galaxies more massive than $3 \cdot 10^{10} M_\odot$ and more luminous than $3.4 \cdot 10^{10} L_{V,\odot}$ (rest-frame) at any z , respectively (Fig. 4). These large limits in M_* and L_V are dictated by the completeness functions required to introduce at different redshifts in order to eliminate the selection effects (Trujillo et al. 2006). In more detail, the predicted radius decrease with z for massive galaxies tends to be steeper than the one inferred from observations up to $z \approx 1$, specially in the V band; for higher redshifts (up to the observational limit of $z = 2.5 - 3$), models and observations agree well.

- Unfortunately, there are not yet available complete high-redshift galaxy samples that would allow to infer the typical stellar and luminous disc size evolution of sub- L_* galaxies. Within the large scatters, our models seem to be consistent with small (not complete) samples of sub- L_* disc galaxies with available rest-frame photometric properties (e.g., Tamm & Tenjes 2006) concerning the measured values of R_B and L_B at different z 's.

The kind of model predictions presented here, unlike previous ones made only on the level of galaxy populations at different redshifts, allow to understand the evolution of individual galaxies and its connection to the properties of the overall galaxy populations. The model predictions are roughly consistent with the currently available observational information on disc size evolution, showing that such an evolution is driven mainly by the Λ CDM halo evolution. The role of some astrophysical mechanisms in play (e.g. mass outflows, late gas infall truncation in massive haloes, stellar and AGN gas re-heating) seems to be of less relevance for the disc

size evolution. More observational inferences are required in order to constrain different models.

ACKNOWLEDGMENTS

We are grateful to the referee for useful comments that have helped to improve the manuscript. V.A.R. thanks PAPIIT-UNAM grant IN114509 and CONACyT grant 60354 for partial funding.

REFERENCES

- Abadi, M. G., Navarro, J. F., Steinmetz, M., & Eke, V. R. 2003, *ApJ*, 591, 499
- Avila-Reese, V., Firmani, C., & Hernández, X. 1998, *ApJ*, 505, 37
- Avila-Reese, V., Firmani, C., Klypin, A., & Kravtsov, A. V. 1999, *MNRAS*, 310, 527
- Avila-Reese, V., & Firmani, C. 2000, *RevMexA&A*, 36, 23
- 2001, *RevMexA&A Conference Series*, 10, 97
- Avila-Reese, V., Zavala, J., Firmani, C., & Hernández-Toledo, H. M. 2008, *AJ*, 136, 1340
- Barden, M., et al. 2005, *ApJ*, 635, 959
- Bett, P., Eke, V., Frenk, C. S., Jenkins, A., Helly, J., & Navarro, J. 2007, *MNRAS*, 376, 215
- Blumenthal, G. R., Faber, S. M., Flores, R., & Primack, J. R. 1986, *ApJ*, 301, 27
- Bouwens, R., & Silk, J. 2002, *ApJ*, 568, 522
- Bouwens, R. J., Illingworth, G. D., Blakeslee, J. P., Broadhurst, T. J., & Franx, M. 2004, *ApJL*, 611, L1
- Bryan, G. L., & Norman, M. L. 1998, *ApJ*, 495, 80
- Bullock, J. S., Dekel, A., Kolatt, T. S., Kravtsov, A. V., Klypin, A. A., Porciani, C., & Primack, J. R. 2001, *ApJ*, 555, 240
- Ceverino, D., & Klypin, A. 2009, *ApJ*, 695, 292
- Cameron, E., & Driver, S. P. 2007, *MNRAS*, 377, 523
- Dutton, A. A., van den Bosch, F. C., Dekel, A., & Courteau, S. 2007, *ApJ*, 654, 27
- Dutton, A. A., & van den Bosch, F. C. 2008, *arXiv:0810.4963*
- Elmegreen, D. M., Elmegreen, B. G., Ravindranath, S., & Coe, D. A. 2007, *ApJ*, 658, 763
- Fall, S. M., & Efstathiou, G. 1980, *MNRAS*, 193, 189
- Firmani, C., & Avila-Reese, V. 2000, *MNRAS*, 315, 457 (FA2000)
- Franx, M., van Dokkum, P. G., Schreiber, N. M. F., Wuyts, S., Labbé, I., & Toft, S. 2008, *ApJ*, 688, 770
- Gnedin, O. Y., Weinberg, D. H., Pizagno, J., Prada, F., & Rix, H.-W. 2007, *ApJ*, 671, 1115
- Governato, F., et al. 2004, *ApJ*, 607, 688
- Governato, F., Willman, B., Mayer, L., Brooks, A., Stinson, G., Valenzuela, O., Wadsley, J., & Quinn, T. 2007, *MNRAS*, 374, 1479
- Graham, A. W., & Worley, C. C. 2008, *MNRAS*, 388, 1708
- Mao, S., Mo, H. J., & White, S. D. M. 1998, *MNRAS*, 297, L71
- Mo, H.J., Mao, S., White, S.D.M. 1998, *MNRAS*, 295,319
- Naab, T., & Ostriker, J. P. 2006, *MNRAS*, 366, 899
- Navarro, J. F., & White, S. D. M. 1994, *MNRAS*, 267, 401
- Peebles, P. J. E. 1969, *ApJ*, 155, 393
- Pizagno, J., et al. 2005, *ApJ*, 633, 844
- Ravindranath, S., et al. 2004, *ApJL*, 604, L9
- Robertson, B., Yoshida, N., Springel, V., & Hernquist, L. 2004, *ApJ*, 606, 32
- Roche, N., Ratnatunga, K., Griffiths, R. E., Im, M., & Naim, A. 1998, *MNRAS*, 293, 157
- Scannapieco, C., Tissera, P. B., White, S. D. M., & Springel, V. 2008, *MNRAS*, 389, 1137
- Schade, D., Lilly, S. J., Crampton, D., Hammer, F., Le Fevre, O., & Tresse, L. 1995, *ApJL*, 451, L1
- Shen, S., Mo, H. J., White, S. D. M., Blanton, M. R., Kauffmann, G., Voges, W., Brinkmann, J., & Csabai, I. 2003, *MNRAS*, 343, 978
- Simard, L., et al. 1999, *ApJ*, 519, 563
- Somerville, R. S., et al. 2008, *ApJ*, 672, 776
- Stringer, M. J., & Benson, A. J. 2007, *MNRAS*, 382, 641
- Tamm, A., & Tenjes, P. 2006, *A&A*, 449, 67
- Trujillo, I., et al. 2004, *ApJ*, 604, 521
- Trujillo, I., et al. 2006, *ApJ*, 650, 18
- van den Bosch, F. C. 2000, *ApJ*, 530, 177
- White, S. D. M., & Rees, M. J. 1978, *MNRAS*, 183, 341
- Zavala, J., Avila-Reese, V., Hernández-Toledo, H., & Firmani, C. 2003, *A&A*, 412, 633
- Zavala, J., Okamoto, T., & Frenk, C. S. 2008, *MNRAS*, 387, 364